PCCP

Plasma-chemical promotion of catalysis for CH4 dry reforming: unveiling plasma-enabled reaction mechanisms

Journal:	*Physical Chemistry Chemical Physics*
Manuscript ID	CP-ART-06-2020-003127.R1
Article Type:	Paper
Date Submitted by the Author:	07-Aug-2020
Complete List of Authors:	Sheng, Zunrong; Tokyo Institute of Technology, Department of Mechanical Engineering Kim, Hyun-Ha; National Institute of Advanced Industrial Science and Technology, Environmental Management Research Institute Yao, Shuiliang; Changzhou University, School of Environmental and Safety Engineering Nozaki, Tomohiro; Tokyo Institute of Technology, Department of Mechanical Engineering

Plasma-chemical promotion of catalysis for CH_4 dry reforming: unveiling plasma-enabled reaction mechanisms

Zunrong Sheng[1], Hyun-Ha Kim[2], Shuiliang Yao[3], Tomohiro Nozaki[1,*]

1 Department of Mechanical Engineering, Tokyo Institute of Technology, Tokyo 152-8550, Japan
2 National Institute of Advanced Industrial Science and Technology, Tsukuba 305-8569, Japan
3 School of Environmental and Safety Engineering, Changzhou University, Changzhou 213164, China

*Corresponding author: Tomohiro Nozaki: nozaki.t.ab@m.titech.ac.jp

Abstract

A kinetic study revealed that a Ni/Al_2O_3 catalyst exhibited a drastic increase in CH_4 and CO_2 conversion under nonthermal plasma when lanthanum was added to the Ni/Al_2O_3 catalyst as a promoter. For a better fundamental understanding of the plasma and catalyst interfacial phenomena, we employed in situ diffuse reflectance infrared Fourier transform spectroscopy (DRIFTS) under plasma-on conditions to elucidate the nonthermal plasma-enabled reaction enhancement mechanisms. Compared with thermal catalysis, plasma-activated CO_2 shows a 1.7-fold enhancement for bidentate (1560 and 1290 cm^{-1}) and monodentate carbonate (1425 and 1345 cm^{-1}) formation on La. Moreover, new peaks of bicarbonate (1655 cm^{-1}) and bridge carbonate (1720 cm^{-1}) were formed due to nonthermal plasma interactions. CO_2-TPD study after plasma- and thermal-activated CO_2 treatment further confirmed that plasma-activated CO_2 enhances bidentate and monodentate carbonate generation with a 1.5-fold promotion at high temperature (500 °C). XRD and EDS analyses suggest that atomic-scale interaction between CO_2-La and CH_x-Ni is possible over the complex La-Ni-Al oxide; vibrationally excited CO_2 ($CO_2^{vib.}$)-induced carbonates provide the key to enhancing the overall performance of CH_4 dry reforming at low temperature.

Keywords

In situ DRIFTS, Plasma-chemical promotion of catalysis, Plasma catalysis, Vibrational excitation, Dry reforming, CO_2 utilization

1. Introduction

Dry methane reforming (DMR) shows significant benefits regarding biogas upgrading to syngas (R1) and reducing greenhouse gas emissions because of accessible and abundant feedstocks [1]. The product syngas is a key chemical feedstock for Fischer-Tropsch upgrading towards high-value products [2, 3].

$$CH_4+CO_2 \rightarrow 2CO+2H_2 \quad \text{R1}$$

However, DMR is an intensive endothermic reaction that requires high-temperature thermal energy [4]. From the perspective of thermodynamics study, spontaneous reaction could not occur at low temperature because a negative Gibbs free energy is required to meet the reaction entropy [5]. To reduce the light-off temperature, nonthermal plasma-assisted reforming is practical with additional electron energy input, which has been demonstrated in some studies [6-8].

From the perspective of kinetic studies, nonthermal plasma-assisted catalysis could reduce the energy barrier by plasma-derived excited species [9-15]. The CH_4 dissociative chemisorption on nickel is considered to be the rate-determining step that controls the overall reaction rate. Our previous study demonstrated that dissociative CH_4 activation on La-modified Ni/Al_2O_3 catalyst was clearly promoted under the influence of nonthermal plasma [16]. We performed comprehensive kinetic analysis, showing that vibrationally excited CH_4 and CO_2 are the key subject [17]. Especially, the role of vibrationally excited CH_4 was investigated by comparing the molecular beam study [18]. Meantime, analysis of plasma-excited CO_2 and their reaction was not well clarified in our previous study [17]. Therefore, we focus on a microscopic study to the deep insight into CO_2 reactivity to form carbonate species, followed by CH_4 reforming.

Regarding the metal-support catalyst (e.g., Ni/Al_2O_3) for DMR, metal nanocrystals are the active sites for CH_4 activation. The interface between the metal and metal oxide is commonly considered the active site for CO_2 activation [19, 20], which inevitably leads to limited active sites for CO_2 activation. Due to the lack of efficient activation sites for plasma-activated CO_2 uptake, a synergistic effect with plasma was not observed clearly in the Ni/Al_2O_3 system [21]. To solve this problem, a promoter and high basic support are expected to improve the performance of CO_2 uptake on the catalyst. The principle is that the basic metal oxide contributes an oxygen anion (O^{2-}) to CO_2 to form a surface carbonate species (CO_3^{2-}), which has been investigated by diffuse reflectance infrared Fourier transform spectroscopy (DRIFTS) on various promoters or supports in thermal catalytic reactions, e.g., CaO [22], TiO_2 [23],

La_2O_3 [24-28], ZrO_2 [29], CeO_2 [30], and MgO [31]. Regarding the plasma-assisted reaction, Ref. [32] demonstrates that the Ni-La_2O_3/$MgAl_2O_4$ catalyst increases the basicity of the catalyst to enhance the chemisorption of CO_2 and further enhance CH_4 activation. However, evidence for an in situ plasma-assisted reaction was not provided. Recently, Xu *et al* reported nonthermal plasma-induced promotion of carbonate, bicarbonate and formate species over a Ru-Mg-Al catalyst surface by in situ DRIFTS-MS study of CO_2 hydrogenation [33]. Other analogical works also presented clear surface activation by plasmas of carbonate and formate species over metal–organic frameworks [34, 35].

To understand the surface intermediates induced by plasma-activated CO_2 on La-modified Ni/Al_2O_3 catalyst, in situ DRIFTS study, under the presence of nonthermal plasma (hereafter in situ plasma-DRIFTS), was employed to reveal CO_2 activation at 200 °C. The CO_2-TPD study was carried out after plasma-activated CO_2 treatment at 500 °C to investigate the amount of adsorbed species compared with that of thermal-activated CO_2 treatment. XRD and EDS were employed to analyze the detailed structure of the catalyst. To reveal the surface reaction between CO_2- and CH_4-derived species, high-temperature in situ DRIFTS without plasma was carried out for a more in-depth mechanistic study.

2. Experimental section

2.1. Catalyst characterization

La-modified Ni/Al_2O_3 catalyst was employed in this study, with the main components of Ni (11 wt%), La (3 wt%) and an Al_2O_3 support, referred to herein as "La-Ni/Al_2O_3". Another catalyst of 12 wt% Ni/Al_2O_3 was employed in this study as a control group without La modification, referred to herein as "Ni/Al_2O_3". A schematic model of Ni/Al_2O_3 is given in another reference [5]. The XRD (Mini Flex 600) analysis of the Ni/Al_2O_3 and La-Ni/Al_2O_3 after thermal H_2 reduction is presented in Figure 1 (a) and (b). The peaks of 44.6 and 51.9 corresponded to Ni(111) and Ni(200), respectively. The mean size of the Ni nanocrystals in Ni/Al_2O_3 was estimated to be 29.0 nm by Scherrer's equation (K=0.94, λ=1.54 Å) based on the average of 8 measurements. Other peaks were assigned to Al_2O_3. In the XRD pattern of La-Ni/Al_2O_3, La_2O_3 was not identified, which has been reported for some La-added catalysts [25, 36-38]. In Figure 1 (b), $LaNiAl_{11}O_{19}$ was identified based on 2θ of 32.1, 34.0, 36.1, 39.3, 42.7, 44.9, 58.5, 60.0 and 67.2° (cf. Figure 1 (c)), illustrating that Ni and La were located on the atomic scale as a complex La-Ni-Al oxide. The structure of $LaNiAl_{11}O_{19}$ is presented in ref [39]. Similarly, the mean size of the Ni crystal of La-Ni/Al_2O_3 was estimated to be 10.8 nm by

Scherrer's equation. In this case, Ni nanocrystals and Ni in the La-Ni-al oxide complex coexisted. Moreover, Figure 1(b) shows peaks of $MgAl_2O_4$ with negligible intensity (0.7 wt% Mg) because Mg-containing dispersing agent was used during the catalyst preparation.

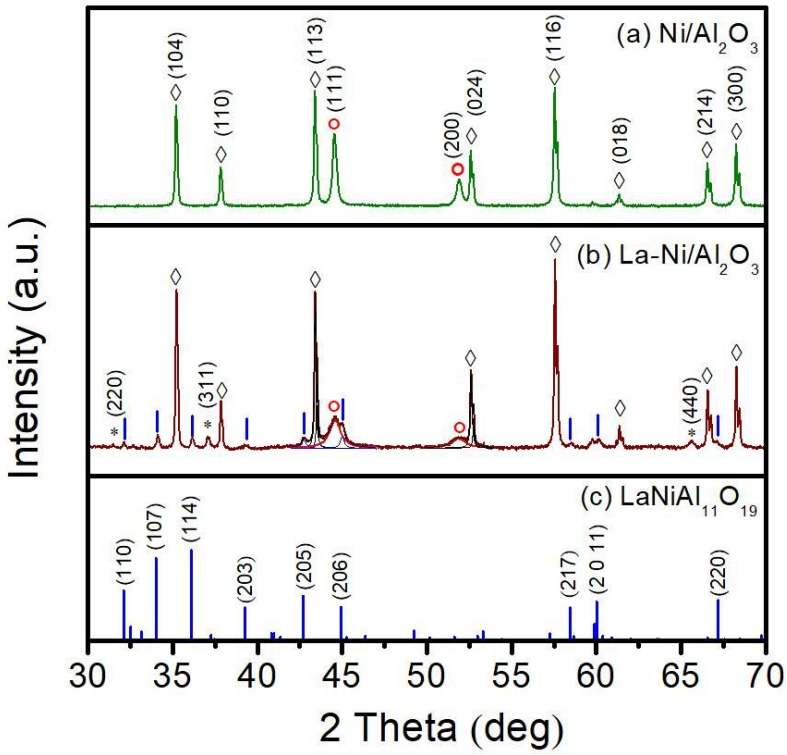

Figure 1. XRD patterns of (a) Ni/Al_2O_3, (b) $La\text{-}Ni/Al_2O_3$, and (c) $LaNiAl_{11}O_{19}$, where ○ Ni; | $LaNiAl_{11}O_{19}$; ◊ Al_2O_3; and ∗ $MgAl_2O_4$.

High-angle annular dark-field STEM (HAADF-STEM) and energy-dispersive X-ray spectroscopy (EDS) (Bruker Nano GmbH) were employed to obtain the nanoparticle images and element distributions. Catalyst pellets were crushed by mechanical milling. Figure 2 (a) and (b) shows HAADF images and Ni mapping of Ni/Al_2O_3, where Ni is identified as distributed nanoparticles in the observation field. The results for $La\text{-}Ni/Al_2O_3$ are shown in Figure 2 (c-f), which presents a different distribution of Ni than Ni/Al_2O_3. First, both Ni nanocrystals and fine Ni (in $LaNiAl_{11}O_{19}$) are detectable in Figure (e), showing a higher and more uniform Ni dispersion than Figure (b). Second and more importantly, Ni and La overlap in Figure (f) due to the combination of (d) and (e). For bimetallic or polymetallic catalysts, the proximity of components is critical for determining the cooperative effect [40]. Synergistic interaction between the active species on Ni and La is highly likely over the La-Ni-Al oxide complex.

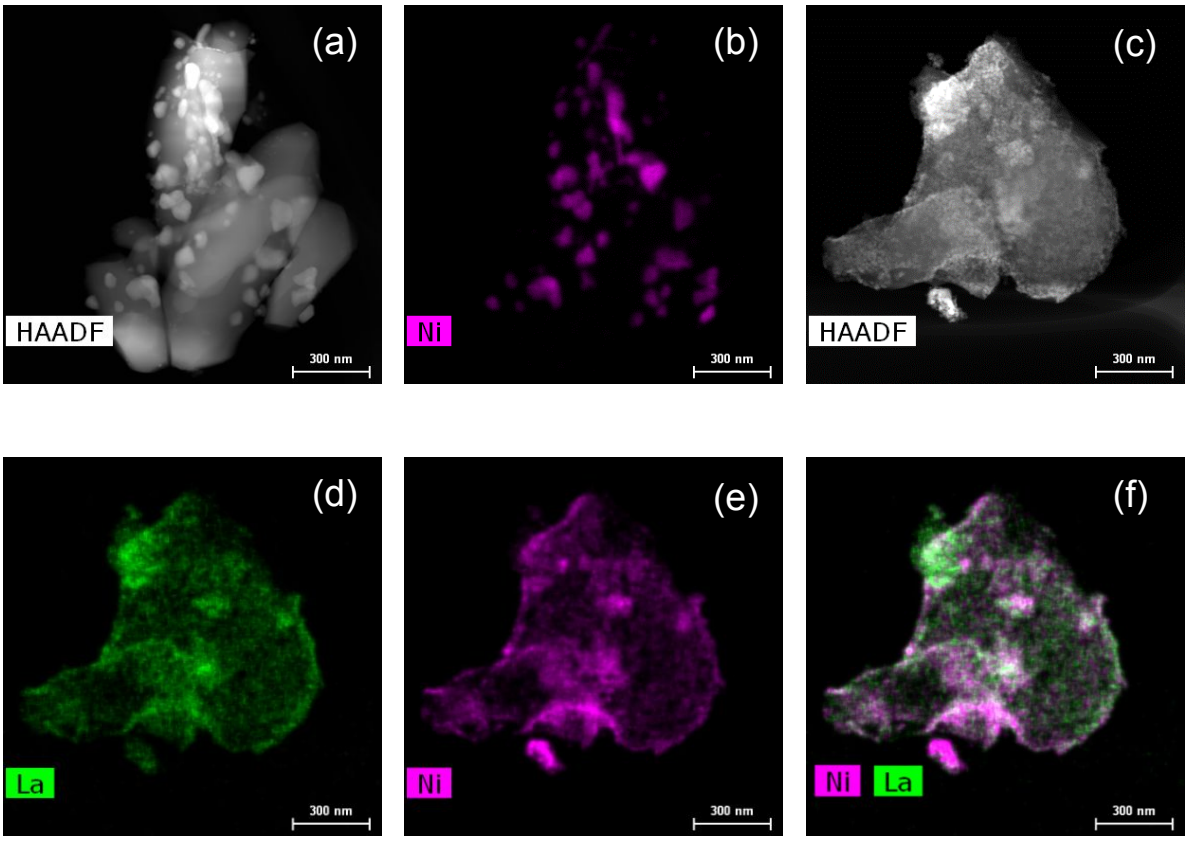

Figure 2. HAADF images and elemental maps: (a and b) Ni/Al_2O_3; (c-f) $La\text{-}Ni/Al_2O_3$.

2.2. In situ DRIFTS

In situ DRIFTS (PerkinElmer Frontier) was employed with a liquid nitrogen-cooled mercury cadmium telluride (MCT) detector. Helium was introduced into the cell as a balance gas with a flow rate of 60 or 100 mL/min. The helium-induced plasma chemistry is discussed in *Supporting information S1*. CH_4/CO_2 was introduced into the cell at 10 mL/min. Two DRIFTS cells were employed: (I) a custom-built plasma-DRIFTS cell (Figure 3) and (II) a high-temperature regular cell without plasma. Figure 3 (a) schematically depicts (I) where a high-voltage needle electrode was located above the catalyst powder (ca. 1 mm gap) to generate a DBD (dielectric barrier discharge)-type nonthermal plasma between the needle and powder. A ground electrode was located at the periphery of the ceramic catalyst holder, which worked as a dielectric barrier. The plasma was generated at a 50 Hz sinusoidal high voltage of 5.5 kV. Figure 3 (b) shows the overall view of the plasma-DRIFTS cell without a catalyst. The top view in Figure 3 (c) shows details of the cell with a 0.1 gram mashed catalyst pellet with a

mean diameter of ca. 1 mm. Figure 3 (d) and (e) shows the emission from the plasma in the visible spectrum. The temperature of the catalyst was maintained at 200 °C during the experiment. The temperature cannot be further increased due to the limitation of heat tolerance: the sealing materials around electrodes could not work at high temperatures (higher than 200 °C). At high temperatures, the gas leakage will occur due to the disorder of sealing materials.

The high-temperature cell (II) has a structure similar to that of the plasma-DRIFTS cell without electrodes, and the temperature of the catalyst can be increased up to 600 °C. Ca. 0.03 g of the powder catalyst filled the holder. Before the experiment, all the catalysts were pretreated by H_2/Ar (100/1000 mL/min) for 60 min at 600 °C in the experimental setup shown in Figure S1 (*Supporting information S2*), the same conditions used in our previous works [16, 21]. All the measurements were taken at atmospheric pressure. The 26-scan accumulation was carried out with a resolution of 4 cm^{-1} for all the spectral recordings.

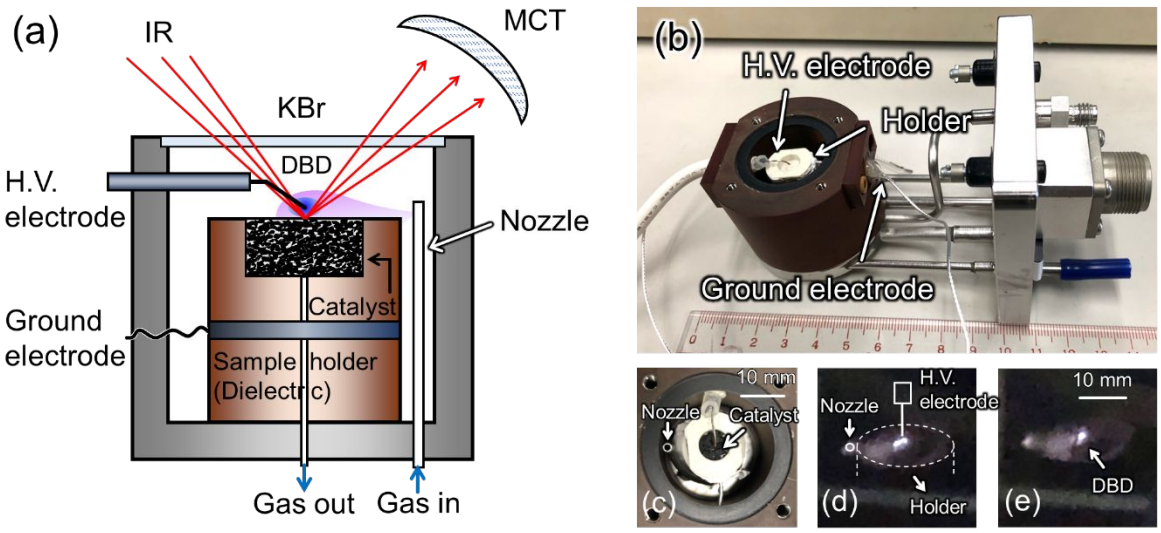

Figure 3. In situ plasma-DRIFTS cell: (a) schematic diagram; (b) overall view; (c) top-view; and (d) and (e) emissions from plasma.

3. Results and discussion

3.1. Enhanced carbonate formation by nonthermal plasma

3.1.1. In situ plasma-DFIFTS study

Figure 4 (a) and (b) shows the spectra from the in situ plasma-DRIFTS cell operated at 200 °C with Ni/Al_2O_3 and $La\text{-}Ni/Al_2O_3$, respectively. Spectrum (a1) in Figure 4 (a) shows the CO_2 activation on Ni/Al_2O_3. The peak in the range of 2260 to 2400 cm^{-1} is assigned to gas

phase CO_2. The broad peaks centered at 1340 and 1600 cm^{-1} are assigned to the generated carbonate species [41, 42], which is presumably on the interface between the Ni nanocrystals and Al_2O_3 [36, 43-45], where adsorption sites are limited due to the small area of the interface. As a result, the absorbance intensity of the peaks of carbonate species is not too strong in the spectrum (a1), showing clear evidence that the interface between Ni and Al_2O_3 supplies weak active sites for CO_2 activation. Spectrum (a2) is obtained after 30 min of treatment with plasma-activated CO_2. Except for the plasma-induced electromagnetic noise, the intensity of the carbonate peaks is not enhanced. Spectrum (a3) is taken when the CO_2 flow and plasma are turned off simultaneously, showing that surface species on Ni/Al_2O_3 was not enhanced after plasma treatment.

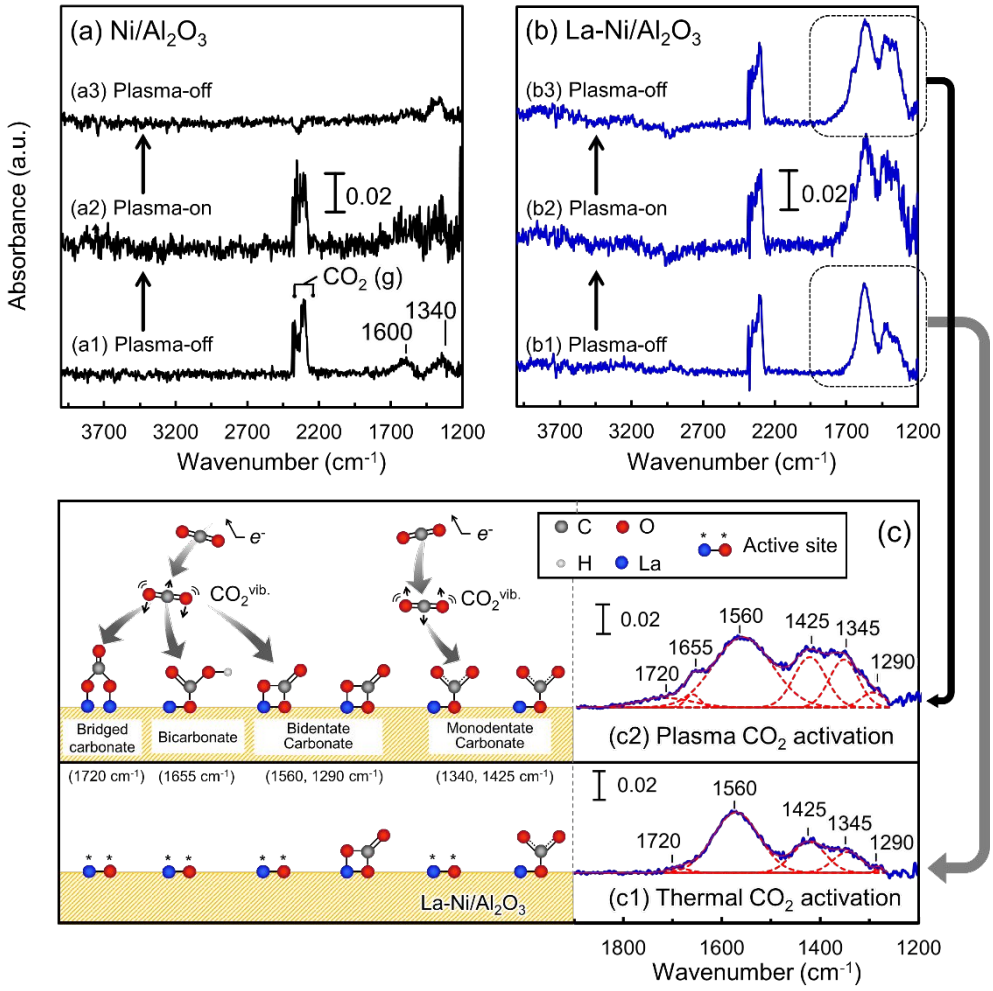

Figure 4. In situ plasma-DRIFTS spectra of CO_2 activation at 200 °C. (a) Ni/Al_2O_3: (a1) 30 min treatment with CO_2/He (9 vol%, 110 mL/min), (a2) 30 min plasma treatment with CO_2/He, and (a3) plasma halt under He flow. (b) La- Ni/Al_2O_3: (b1) 40 min treatment with CO_2/He, (b2) 30 min plasma treatment with CO_2/He, and (b3) plasma halt under CO_2/He flow. (c) shows the vibrationally excited CO_2-enhanced mechanism of carbonate formation

accompanied by magnified spectra (c1 and c2).

The spectra in Figure 4 (b) represent La-Ni/Al_2O_3. The overlapping peaks between 1200 and 1800 cm^{-1} are assigned to several carbonate species [44, 46]. The details of all the carbonate species coordinated with La are summarized in *Supporting information S3*. Spectrum (b1) is obtained when the CO_2 activation reaches steady state with 40 min of treatment. Figure 4 (c1) shows magnified carbonate peaks, which are deconvoluted to several peaks as the red dashed curves. The peaks centered at 1560 cm^{-1} and 1290 cm^{-1} are assigned to bidentate carbonate [36]. The peaks at 1425 and 1345 cm^{-1} are assigned to monodentate carbonate [36, 47, 48]. A broad peak at 1720 cm^{-1} is assigned to bridged carbonate [22] at a negligible intensity. The intensity of the carbonate peaks is much stronger than that of Ni/Al_2O_3 in spectrum (a1), illustrating that complex La-Ni-Al oxide works as the active site for CO_2 activation. It must be mentioned that the dispersing agent, Mg oxide species, may has an effect on CO_2 activation although the content is low (0.7 wt%). However, the deconvolution of such influence is impracticable in DRIFTS spectra where the CO_2-La (or carbonate-La) system is unambiguously established based on the higher content of La (3 wt%), uniform dispersion, and literature support. We should not discard any possibility of the influence of Mg species hidden behind the DRIFTS data, which is expected to be investigated in the future work with optimized catalyst preparation technology.

The spectrum (b2) in Figure 4 (b) is obtained under plasma treatment. Due to the electromagnetic noise in spectrum (b2), the spectrum (b3) is shown to highlight the plasma-induced changes. The spectrum (b3) is magnified in Figure (c2), where the bidentate and monodentate carbonate contents are clearly increased after plasma treatment: the total areas of peaks of bidentate carbonate (1560 and 1290 cm^{-1}) and monodentate carbonate (1425 and 1345 cm^{-1}) in plasma-activated CO_2 activation (Figure (c2)) show an approximately 1.7-fold enhancement compared to those of thermal-activated CO_2 (Figure (c1)). In addition, bridged carbonate (1720 cm^{-1}) [22] and bicarbonate (also called hydrogen carbonate) (1655 cm^{-1}) [24, 48, 49] are generated. The broad peak centered at 3800 cm^{-1} may be attributed to the OH band of bicarbonate [27, 31, 50]. The surface hydrogen species from catalyst pretreatment (thermal H_2 reduction) may contribute the hydrogen species for generating bicarbonate with plasma.

Electron collision kinetic analysis reveals that the production of vibrationally excited species in nonthermal plasma is the dominant reaction pathway rather than dissociation and ionization when the reduced electric field (E/N) is low [16, 17]. As discussed in *Supporting information S1*, helium would increase electron number density via the reaction by metastable species, but mean electron energy and thus electron collision kinetics would not change to a

large extent. Energy loss fraction analysis showed that a large part of electrical energy is consumed by dissociation and ionization of molecules in DBD type nonthermal plasma [51]. Meantime, comparison of inelastic collision frequency in DBD shows clearly that production of vibrationally excited CO_2 becomes the dominant pathway than CO_2 dissociation to CO [16, 17]. Eq. 1 shows that vibrationally excited molecules are produced due to low energy electron impact with a rate constant k_v. Here, A represents a neutral molecule such as CO_2 or CH_4. The rate expression for the production of vibrationally excited species is formulated in Eq. 2, where N_A and N_e represent the number densities of neutral molecules and electrons, respectively. Our previous study demonstrated that the production of vibrationally excited CO_2 and CH_4 is 40-150 times greater than the electron number density, as shown in Eq. 3 [16, 52]. In other words, a single electron produces 40 to 150 times more vibrationally excited molecules. Therefore, the vibrationally excited species is the most abundant species in the nonthermal plasma environment. A molecular beam study revealed that vibrational excitation is effective at promoting the reaction between the incident molecule and catalyst surface [53], contributing to the enhanced surface coverage of adsorbed species by vibrational energy redistribution [18, 54].

We highlight that plasma-induced vibrationally excited CO_2 plays a key role in enhanced carbonate formation over La-Ni/Al_2O_3, which is schematically depicted in Figure 4 (c): (c1) shows that active sites in complex La-Ni-Al oxide are occupied by carbonates in thermal-activated CO_2 activation. When plasma-activated CO_2 treatment starts, electron-induced vibrationally excited CO_2 has a stronger interaction with unoccupied active sites. Consequently, bridged carbonate and bicarbonate are generated, and the formation of monodentate and bidentate carbonate is enhanced, as shown in Figure (c2). It should be pointed out that CO_2 dissociation products, i.e. CO and O radical, cannot generate carbonate species (CO_3^{2-}). Moreover, gas phase CO band and adsorbed CO band were absent during CO_2 treatment with plasma-on in Figure 4.

$$A + e \xrightarrow{k_v} A^v + e \qquad \text{Eq. 1}$$

$$r_v = \frac{\mathrm{d}N_A^v}{\mathrm{d}t} = k_v N_A N_e \qquad \text{Eq. 2}$$

$$N_A^v = (40 - 150) N_e \qquad \text{Eq. 3}$$

3.1.2. Ex situ CO_2-TPD study

The plasma-DRIFTS experiments present carbonate generation behavior at 200 °C due to the limitation of heat tolerance of the plasma-DRIFTS chamber. To investigate carbonate generation at high temperatures, CO_2-TPD (temperature programmed desorption) was carried out after CO_2 treatment with and without plasma. The details of the CO_2-TPD experiment are presented in *Supporting information S2,* and the setup is depicted in Figure S1. The TPD patterns of Ni/Al_2O_3 are shown in Figure S2, where the CO_2 desorption (signal of m/e=44) is negligibly weak in patterns (a) and (b), illustrating that the carbonate generation over Ni/Al_2O_3 is intrinsically weak. Plasma-enhanced synergism is not observed clearly for Ni/Al_2O_3 catalysts, which correlates well with the DRIFTS experiments shown in Figure 4 (a).

The results for La-Ni/Al_2O_3 are shown in Figure 5. All the curves between 300 and 600 °C are deconvoluted into several peaks, and the fitting curve (an orange dotted line) overlaps with the original spectrum. The curve (a) in Figure 5 is the CO_2-TPD pattern after thermal CO_2 treatment. The assignment of peaks I-IV are summarized in Table 1. Peaks I and II are attributed to the desorption of the bidentate carbonate adsorbed on the interface between Ni and Al_2O_3 (hereafter Al_2O_3) and the La in the La-Ni-Al oxide complex (hereafter La) [36], respectively. The desorption temperature of carbonate at different sites can be distinguished based on the premise that La oxide is more basic than Al_2O_3 [55-57], which leads to a higher desorption temperature. Peaks III and IV at higher temperatures correspond to the desorption of monodentate carbonate absorbed on Al_2O_3 and La, respectively [36]. A comparison between the TPD peaks of La-Ni/Al_2O_3 and Ni/Al_2O_3 (*supporting informing Figure S2*) shows that peaks I (I') and III (III') are common features of these two catalysts, which are related to Al_2O_3. However, peaks II and IV are unique features of La-Ni/Al_2O_3. Compared with thermal CO_2 treatment, peaks II, III and IV are enhanced after plasma CO_2 treatment in Figure 5, which corresponds well with the DRIFTS results at low temperature. Here, we conclude that plasma CO_2 at high and low temperatures can enhance carbonate generation over La-Ni/Al_2O_3.

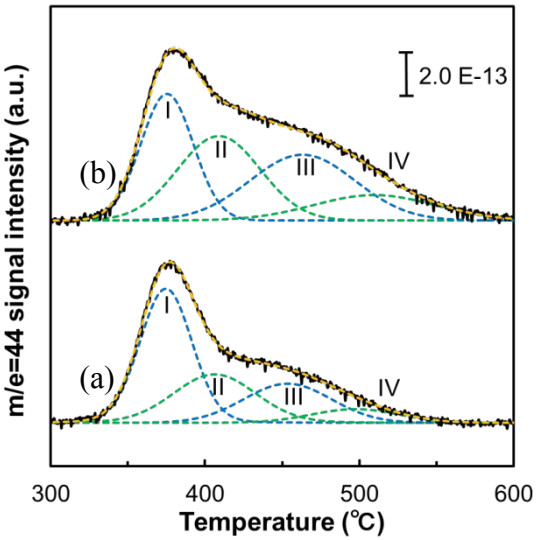

Figure 5. CO_2-TPD patterns of La-Ni/Al_2O_3 after 500 °C treatment: (a) thermally activated CO_2 and (b) plasma-activated CO_2. The CO_2 flow rate was 500 mL/min at 10 kPa. The heating rate was 10 °C/min.

Table 1. The assignment of peak I–IV for La-Ni/Al_2O_3.

Peak	Temp. (°C)	Carbonate type	Active site
I	375	Bi-	Al_2O_3
II	400	Bi-	La
III	460	Mono-	Al_2O_3
IV	500	Mono-	La

Remarks: Bi- and Mono- are abbreviations of bicarbonate and monodentate, respectively; Al_2O_3 represents the interface between Ni and Al_2O_3, and La represents complex La-Ni-Al oxide.

3.2. Carbonate-induced reaction pathway for DMR enhancement

3.2.1. In situ DRIFTS study

The carbonate generation over La-Ni/Al_2O_3 is clearly enhanced by CO_2 plasma at 200 °C. Meanwhile, Ni/Al_2O_3 without La is inert for carbonate generation. CH_4 activation is difficult at 200 °C even with plasma (cf. *Supporting information S4*): therefore, reaction between carbonates and CH_4 over La-Ni/Al_2O_3 was studied by high temperature DRIFTS (600 °C). Note, due to the limitation of heat tolerance of plasma-DRIFTS chamber, the experiments were carried out using regular DRIFTS chamber without plasma application. There are two steps in this experiment: (i) CO_2 treatment; (ii) CH_4 treatment over carbonate-containing catalyst.

The spectrum at 1 min in Figure 6 (a) for CO_2 treatment shows two broad peaks centered at 1560 cm^{-1} and 1354 cm^{-1}, which are assigned to bidentate and monodentate carbonates, respectively. Then, the CO_2 flow is switched to CH_4 at 2 min. Gas phase CH_4 is detected as peaks at 1304, 1354 and 3015 cm^{-1} (not shown). With continuous CH_4 flow, the peak at 1560 cm^{-1} shifts gradually to 1500 cm^{-1} between 2 and 4 min because the bidentate carbonate (1560 cm^{-1}) is gradually consumed, while polydentate carbonate (1500 cm^{-1}) [24, 58] becomes dominant, indicating that bidentate carbonate reacts primarily with CH_4-derived species. Additionally, a weak broad band centered at 1750 cm^{-1} appears when CH_4 is introduced, which

is assigned to the C=O stretching vibration in surface CH_xO^* (x=1-3) species [59-61], and it is expected as the intermediate species for generating CO and H_2 [62, 63]. Here, the adsorbed species are denoted by "*". In this case, the CH_x^* from CH_4 dehydrogenation is continuously oxidized by CO_3^{2-} (bidentate carbonate) to generate CH_xO^* before complete dehydrogenation to coke formation occurs. The peaks of gas phase CO (2113 and 2176 cm^{-1} [64]) are detectable at 4.5 min accompanied by an enhanced CH_xO^* band (1750 cm^{-1}), indicating that the successful production of CH_xO^* leads to syngas (CO and H_2) generation.

In Figure 6 (b), the bands of product CO (g) became weak at 5 min due to the carbonate species being consumed, which is confirmed by the fact that all the carbonate peaks (between 1200 and 1800 cm^{-1}) disappear. The lack of carbonates leads to the oxidation-reduction behavior of Ni [23], which is attributed to the baseline shift from 5 to 7 min. *Supporting information S5* demonstrates the transmittance difference between the reduced and oxidized samples, as well as the oxidation-reduction behavior. CH_4 is dehydrogenated continuously to coke [44] after the carbonates are fully consumed. The CH_4 flow is turned off at 8 min, and all the carbonate bands disappear.

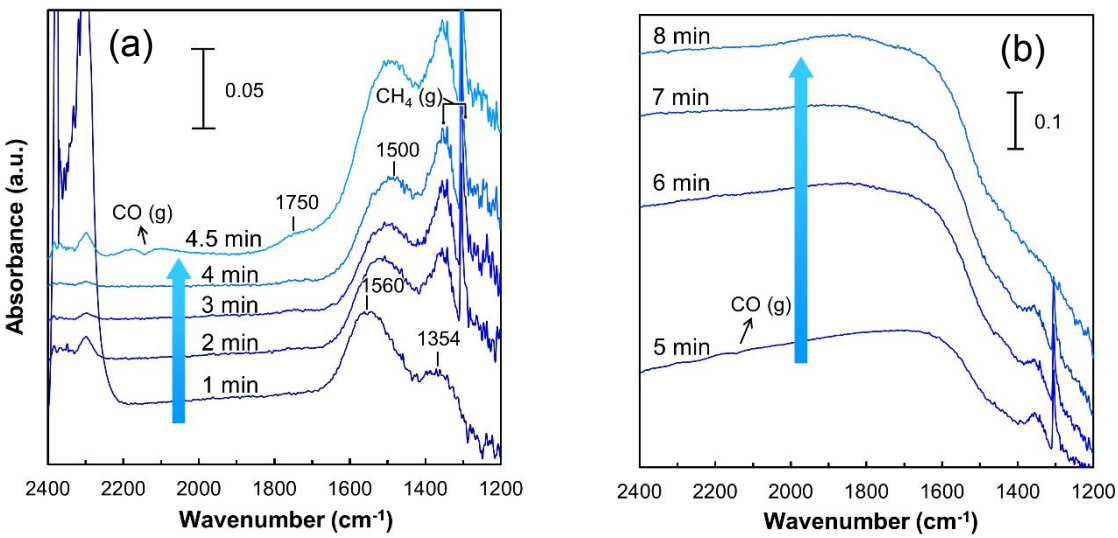

Figure 6. In situ DRIFTS spectra of CH_4 flows to carbonate-containing La-Ni/Al_2O_3 at 600 °C (plasma-off). 1 min: CO_2/He=14 vol %, 70 mL/min; 2-7 min: CH_4/He=14 vol %, 70 mL/min; 8 min: He=60 mL/min.

3.2.2. Relationship between carbonate formation and CH_4 conversion

Table 2 summarizes the CH_4 conversion from our previous works [16, 21], as well as the amounts of carbonates obtained from the DRIFTS and CO_2-TPD results. For Ni/Al_2O_3, CH_4 conversion is not increased under plasma reforming compared with that of thermal reforming

[21], indicating that the plasma-induced synergism for CH_4 conversion is negligible. For La-Ni/Al_2O_3, plasma reforming shows a 1.5-fold enhancement in CH_4 conversion compared with thermal reforming [16]. Meanwhile, the enhancement of carbonate formation by plasma is 1.5-1.8 times greater than thermal catalysis: it is noteworthy that there is a good correlation between CH_4 conversion and carbonate formation enhancement behavior.

In the case of Ni/Al_2O_3, Ni forms nanoparticles providing the active sites for CH_4 dissociative chemisorption. On the other hand, in the case of La-Ni/Al_2O_3, Ni is consumed for Ni nanoparticles and La-Ni-Al oxide which provides peculiar active sites for carbonate formation. The Ni weight percent of Ni/Al_2O_3 (12% wt.) is higher than that of La-Ni/Al_2O_3 (11% wt.). Moreover, approximately 2% wt. Ni contributes to $LaNiAl_{11}O_{19}$, while 9% wt. Ni nanoparticles are estimated in La-Ni/Al_2O_3. Therefore, the CH_4 conversion with La-Ni/Al_2O_3 is lower than that with Ni/Al_2O_3. Another possibility is that active site for CH_4 chemisorption is interrupted by carbonate formation. Because reaction order for CO_2 takes negative value for the forward CH_4 reaction rate equation [17]: as CO_2 partial pressure increases, CH_4 conversion decreases.

Table 2. Comparison of the CH_4 conversion and amount of carbonate generated

	CH_4 conversion in DMR		Amount of carbonate generated	
Reference	Kameshima S. *et al* [21] (*a)	Sheng Z. *et al* [16] (*b)	DRIFTS results in Figure 4 (c) (*c)	CO_2-TPD results in Figure 5 (*d)
Catalyst	Ni/Al_2O_3	La-Ni/Al_2O_3		
Unit	mL/min	mL/min	Areal intensity of absorbance (-)	Areal intensity of desorbed-CO_2 (-)
Thermal	450	141	8.3	5.6
Plasma	450	204	14.9	8.3
Gain	1	1.5	1.8	1.5
Remarks	(*a) Catalyst temperature=600 °C; flow rate of CH_4/CO_2=1000 mL/min; catalyst weight=14 g. (*b) Catalyst temperature=600 °C; flow rate of CH_4/CO_2=500 mL/min; catalyst weight=11 g. (*c) Areal intensity of absorbance from DRIFTS was calculated by integration of absorbance intensity (a.u.) with wavenumber (cm^{-1}). (*d) Areal intensity of desorbed-CO_2 was calculated by integration of current intensity of m/z=44 (a.u.) with time (min).			

3.2.3. Reaction mechanism of plasma-enhanced DMR

The plasma-enhanced reaction pathways over La-Ni/Al_2O_3 are explained based on the Langmuir-Hinshelwood mechanism, which are schematically illustrated in Figure 7. First, CH_4 is dissociatively chemisorbed on Ni as CH_3^* and H^* (R2), followed by consecutive dehydrogenation of adsorbed CH_3^* to fragments (CH_x^*) (R3). Additionally, as an acidic species, CO_2 is adsorbed and activated on La because the La in the La-Ni-Al oxide supports a basic site contributing anionic oxygen (O^{2-}) to adsorbed CO_2 for surface covalent carbonate species (CO_3^{2-}) formation (R4). At the initial stage of reforming, vibrationally excited CH_4 and CO_2 enhance the interaction with catalysts, contributing to the increased amount of surface species.

$$CH_4 + * \rightarrow CH_3^* + H^* \quad \text{R2}$$

$$CH_3^* \rightarrow CH_x^* + (3\text{-}x)\ H^*\ (x=1, 2) \quad \text{R3}$$

$$CO_2 + O^{2-} \rightarrow CO_3^{2-} \quad \text{R4}$$

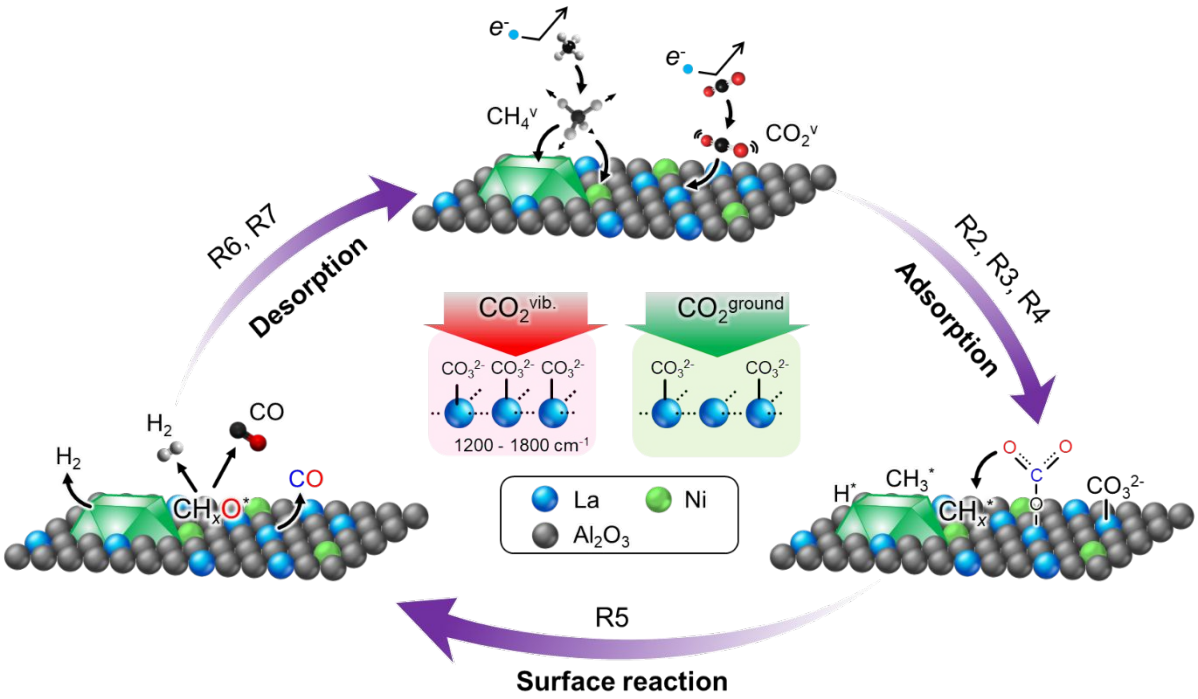

Figure 7. Plasma enhanced reaction pathways over La-Ni/Al_2O_3.

In the second stage of reforming, carbonate species (CO_3^{2-}) oxidize CH_x^* (x=1-3) quickly on adjacent Ni to form CH_xO^* (R5), and successful production of CH_xO^* leads to syngas (CO and H_2) production (R6 and R7): as a result, active sites of Ni for CH_4 adsorption are regenerated. In this case, complete dehydrogenation of CH_3^* to carbon, i.e., coking, is inhibited.

More carbonate generation by plasma-activated CO_2 is expected to accelerate the surface reaction (R5) by increasing the surface coverage of carbonate. As a result, a promoted CH_4 conversion in plasma-assisted reforming is observed, as summarized in Table 2.

$CO_3^{2-} + CH_x^* \rightarrow CH_xO^* + CO + O^{2-}$ (x=1-3) R5

$CH_xO^* \rightarrow CO + x/2\ H_2 + *$ R6

$H^* + H^* \rightarrow H_2 + *$ R7

Likewise, plasma-activated CH_4 is anticipated to promote dissociative chemisorption over Ni sites. However, CH_x^* fragments need to react with carbonate species, and the active sites must be regenerated for the successive CH_4 conversion to syngas. This is presumably the reason that the interaction between plasma-generated active species and Ni/Al_2O_3 is weak without La.

In addition to abovementioned mechanism, there is a possibility of Eley-Rideal (E-R) mechanism where CO_2^v react with adsorbed CH_x^*, leading to syngas production. Quan *et al* have performed the molecular beam study (ultra-high vacuum and cryogenic temperature) for the detection of reaction between vibrationally excited CO_2 and adsorbed H_2 within the scope of E-R mechanism [53]. Based on this fact, we should not discard the possibility of E-R mechanism which may occur parallel to carbonate formation in the plasma-catalyst system. However, it is hard to identify the E-R mechanism by the given in situ plasma-DRIFTS approach. We might be able to identify the E-R mechanism in our system, but we need a careful design of the experimental apparatus which is not necessarily limited to plasma-DRIFTS. Therefore, E-R mechanism is not included in Figure 7, because the experimental evidence is missing for now.

4. Conclusion

Nonthermal plasma can enhance CO_2 activation on La, leading to more surface carbonate species formation than with thermal catalysis. Moreover, bicarbonate and bridge carbonate can be generated by plasma treatment. Due to the characteristics of the neighboring distribution on the atomic scale between Ni and La in the La-Ni-Al oxide complex, the CO_2-La-derived carbonate species can oxidize CH_x^* on Ni to generate syngas. The synergism of plasma-assisted reforming is explained by the plasma-enhanced surface carbonate generation: more surface carbonates contribute to a higher surface coverage of CO_2. The faster surface reaction between CH_x^* species and carbonates leads to higher CH_4 conversion in plasma-assisted dry methane

reforming. We would like to point out that activation of CH_4 into vibrational states should also play a vital role; however, coreactants, i.e., plasma-activated CO_2, that form surface carbonates are necessary to maximize plasma catalysis.

Conflicts of interest

There are no conflicts to declare.

Acknowledgements

This project is supported by JST CREST (JPMJCR19R3) and KAKENHI (18H01208). Z.S. acknowledges the financial support from the program of China Scholarships Council (Grant No. 201707040056).

References

[1] S.N.B. Villadsen, P.L. Fosbøl, I. Angelidaki, J.M. Woodley, L.P. Nielsen, P. Møller, The Potential of Biogas; the Solution to Energy Storage, ChemSusChem 12 (2019) 2147-2153.

[2] R.G. Grim, A.T. To, C.A. Farberow, J.E. Hensley, D.A. Ruddy, J.A. Schaidle, Growing the Bioeconomy through Catalysis: A Review of Recent Advancements in the Production of Fuels and Chemicals from Syngas-Derived Oxygenates, ACS Catalysis 9 (2019) 4145-4172.

[3] P.J. Woolcock, R.C. Brown, A review of cleaning technologies for biomass-derived syngas, Biomass and Bioenergy 52 (2013) 54-84.

[4] S. Liu, L.R. Winter, J.G. Chen, Review of Plasma-Assisted Catalysis for Selective Generation of Oxygenates from CO2 and CH4, ACS Catalysis 10 (2020) 2855-2871.

[5] S. Zunrong, K. Seigo, S. Kenta, N. Tomohiro, In Plasma Chemistry and Gas Conversion; Britum,N., Silva,T.,Eds.; IntechOpen: London, 2018, p 37-57.

[6] X. Wang, Y. Gao, S. Zhang, H. Sun, J. Li, T. Shao, Nanosecond pulsed plasma assisted dry reforming of CH4: The effect of plasma operating parameters, Applied Energy 243 (2019) 132-144.

[7] L. Wang, Y. Yi, C. Wu, H. Guo, X. Tu, One-Step Reforming of CO2 and CH4 into High-Value Liquid Chemicals and Fuels at Room Temperature by Plasma-Driven Catalysis, Angewandte Chemie 56 (2017) 13679-13683.

[8] S. Kameshima, R. Mizukami, T. Yamazaki, L.A. Prananto, T. Nozaki, Interfacial reactions between DBD and porous catalyst in dry methane reforming, Journal of Physics D: Applied Physics 51 (2018) 114006.

[9] S. Xu, S. Chansai, C. Stere, B. Inceesungvorn, A. Goguet, K. Wangkawong, S.F.R. Taylor, N. Al-Janabi, C. Hardacre, P.A. Martin, X. Fan, Sustaining metal–organic frameworks for water–gas shift catalysis by non-thermal plasma, Nature Catalysis 2 (2019) 142-148.

[10] S. K. P. Veerapandian, N. De Geyter, J.-M. Giraudon, J.-F. Lamonier, R. Morent, The Use of Zeolites for

VOCs Abatement by Combining Non-Thermal Plasma, Adsorption, and/or Catalysis: A Review, Catalysts 9 (2019).

[11] J.C. Whitehead, Plasma–catalysis: the known knowns, the known unknowns and the unknown unknowns, Journal of Physics D: Applied Physics 49 (2016) 243001.

[12] E.C. Neyts, A. Bogaerts, Understanding plasma catalysis through modelling and simulation—a review, Journal of Physics D: Applied Physics 47 (2014) 224010.

[13] J. Kim, D.B. Go, J.C. Hicks, Synergistic effects of plasma-catalyst interactions for CH4 activation, Physical chemistry chemical physics : PCCP 19 (2017) 13010-13021.

[14] H.L. Chen, H.M. Lee, S.H. Chen, Y. Chao, M.B. Chang, Review of plasma catalysis on hydrocarbon reforming for hydrogen production—Interaction, integration, and prospects, Applied Catalysis B: Environmental 85 (2008) 1-9.

[15] E.C. Neyts, K. Ostrikov, M.K. Sunkara, A. Bogaerts, Plasma Catalysis: Synergistic Effects at the Nanoscale, Chemical Reviews 115 (2015) 13408-13446.

[16] Z. Sheng, K. Sakata, Y. Watanabe, S. Kameshima, H.-H. Kim, S. Yao, T. Nozaki, Factors determining synergism in plasma catalysis of biogas at reduced pressure, Journal of Physics D: Applied Physics 52 (2019) 414002.

[17] Z. Sheng, Y. Watanabe, H.-H. Kim, S. Yao, T. Nozaki, Plasma-enabled mode-selective activation of CH4 for dry reforming: First touch on the kinetic analysis, Chemical Engineering Journal 399 (2020) 125751.

[18] A.L. Utz, Mode selective chemistry at surfaces, Current Opinion in Solid State and Materials Science 13 (2009) 4-12.

[19] L. Foppa, T. Margossian, S.M. Kim, C. Müller, C. Copéret, K. Larmier, A. Comas-Vives, Contrasting the Role of Ni/Al2O3 Interfaces in Water–Gas Shift and Dry Reforming of Methane, Journal of the American Chemical Society 139 (2017) 17128-17139.

[20] M.-C. Silaghi, A. Comas-Vives, C. Copéret, CO2 Activation on Ni/γ–Al2O3 Catalysts by First-Principles Calculations: From Ideal Surfaces to Supported Nanoparticles, ACS Catalysis 6 (2016) 4501-4505.

[21] S. Kameshima, K. Tamura, R. Mizukami, T. Yamazaki, T. Nozaki, Parametric analysis of plasma-assisted pulsed dry methane reforming over Ni/Al2O3 catalyst, Plasma Processes and Polymers 14 (2017) 1600096.

[22] D.A. Constantinou, A.M. Efstathiou, The steam reforming of phenol over natural calcite materials, Catalysis Today 143 (2009) 17-24.

[23] M.C.J. Bradford, M. Albert Vannice, The role of metal–support interactions in CO2 reforming of CH4, Catalysis Today 50 (1999) 87-96.

[24] S.C. Shen, X. Chen, S. Kawi, CO2 Adsorption over Si-MCM-41 Materials Having Basic Sites Created by Postmodification with La2O3, Langmuir 20 (2004) 9130-9137.

[25] L. Qian, Z. Ma, Y. Ren, H. Shi, B. Yue, S. Feng, J. Shen, S. Xie, Investigation of La promotion mechanism on Ni/SBA-15 catalysts in CH4 reforming with CO2, Fuel 122 (2014) 47-53.

[26] O.V. Manoilova, S.G. Podkolzin, B. Tope, J. Lercher, E.E. Stangland, J.-M. Goupil, B.M. Weckhuysen, Surface Acidity and Basicity of La2O3, LaOCl, and LaCl3 Characterized by IR Spectroscopy, TPD, and DFT Calculations, The Journal of Physical Chemistry B 108 (2004) 15770-15781.

[27] X.E. Verykios, Catalytic dry reforming of natural gas for the production of chemicals and hydrogen, International Journal of Hydrogen Energy 28 (2003) 1045-1063.

[28] J.F. Múnera, S. Irusta, L.M. Cornaglia, E.A. Lombardo, D. Vargas Cesar, M. Schmal, Kinetics and reaction pathway of the CO2 reforming of methane on Rh supported on lanthanum-based solid, Journal of Catalysis 245 (2007) 25-34.

[29] K. Pokrovski, K.T. Jung, A.T. Bell, Investigation of CO and CO2 Adsorption on Tetragonal and Monoclinic Zirconia, Langmuir 17 (2001) 4297-4303.

[30] T. Tabakova, F. Boccuzzi, M. Manzoli, D. Andreeva, FTIR study of low-temperature water-gas shift reaction on gold/ceria catalyst, Applied Catalysis A: General 252 (2003) 385-397.

[31] D. Cornu, H. Guesmi, J.-M. Krafft, H. Lauron-Pernot, Lewis Acido-Basic Interactions between CO2 and MgO Surface: DFT and DRIFT Approaches, The Journal of Physical Chemistry C 116 (2012) 6645-6654.

[32] A.H. Khoja, M. Tahir, N.A. Saidina Amin, Evaluating the Performance of a Ni Catalyst Supported on La2O3-MgAl2O4 for Dry Reforming of Methane in a Packed Bed Dielectric Barrier Discharge Plasma Reactor, Energy & Fuels 33 (2019) 11630-11647.

[33] S. Xu, S. Chansai, Y. Shao, S. Xu, Y.-c. Wang, S. Haigh, Y. Mu, Y. Jiao, C.E. Stere, H. Chen, X. Fan, C. Hardacre, Mechanistic study of non-thermal plasma assisted CO2 hydrogenation over Ru supported on MgAl layered double hydroxide, Applied Catalysis B: Environmental 268 (2020) 118752.

[34] H. Chen, Y. Mu, Y. Shao, S. Chansai, H. Xiang, Y. Jiao, C. Hardacre, X. Fan, Nonthermal plasma (NTP) activated metal–organic frameworks (MOFs) catalyst for catalytic CO2 hydrogenation, AIChE Journal 66 (2020) e16853.

[35] R. Vakili, R. Gholami, C.E. Stere, S. Chansai, H. Chen, S.M. Holmes, Y. Jiao, C. Hardacre, X. Fan, Plasma-assisted catalytic dry reforming of methane (DRM) over metal-organic frameworks (MOFs)-based catalysts, Applied Catalysis B: Environmental 260 (2020) 118195.

[36] K. Li, X. Chang, C. Pei, X. Li, S. Chen, X. Zhang, S. Assabumrungrat, Z.-J. Zhao, L. Zeng, J. Gong, Ordered mesoporous Ni/La2O3 catalysts with interfacial synergism towards CO2 activation in dry reforming of methane, Applied Catalysis B: Environmental 259 (2019) 118092.

[37] K. Sutthiumporn, S. Kawi, Promotional effect of alkaline earth over Ni–La2O3 catalyst for CO2 reforming of CH4: Role of surface oxygen species on H2 production and carbon suppression, International Journal of Hydrogen Energy 36 (2011) 14435-14446.

[38] W. Mo, F. Ma, Y. Ma, X. Fan, The optimization of Ni–Al2O3 catalyst with the addition of La2O3 for CO2–CH4 reforming to produce syngas, International Journal of Hydrogen Energy 44 (2019) 24510-24524.

[39] M. Gasperin, M.C. Saine, A. Kahn, F. Laville, A.M. Lejus, Influence of M2+ ions substitution on the structure of lanthanum hexaaluminates with magnetoplumbite structure, Journal of Solid State Chemistry 54 (1984) 61-69.

[40] A. Tou, H.-H. Kim, H. Einaga, Y. Teramoto, A. Ogata, Ozone-assisted catalysis of CO: In situ Fourier transform IR evidence of the cooperative effect of a bimetallic Ag-Pd catalyst, Chemical Engineering Journal 355 (2019) 380-389.

[41] K.K. Bando, K. Sayama, H. Kusama, K. Okabe, H. Arakawa, In-situ FT-IR study on CO2 hydrogenation

over Cu catalysts supported on SiO2, Al2O3, and TiO2, Applied Catalysis A: General 165 (1997) 391-409.

[42] A. Karelovic, P. Ruiz, Improving the Hydrogenation Function of Pd/γ-Al2O3 Catalyst by Rh/γ-Al2O3 Addition in CO2 Methanation at Low Temperature, ACS Catalysis 3 (2013) 2799-2812.

[43] A. Slagtern, Y. Schuurman, C. Leclercq, X. Verykios, C. Mirodatos, Specific Features Concerning the Mechanism of Methane Reforming by Carbon Dioxide over Ni/La2O3Catalyst, Journal of Catalysis 172 (1997) 118-126.

[44] S. Jiang, Y. Lu, S. Wang, Y. Zhao, X. Ma, Insight into the reaction mechanism of CO2 activation for CH4 reforming over NiO-MgO: A combination of DRIFTS and DFT study, Applied Surface Science 416 (2017) 59-68.

[45] Z. Sheng, S. Kameshima, S. Yao, T. Nozaki, Oxidation behavior of Ni/Al2O3 catalyst in nonthermal plasma-enabled catalysis, Journal of Physics D: Applied Physics 51 (2018) 445205.

[46] M. Németh, Z. Schay, D. Srankó, J. Károlyi, G. Sáfrán, I. Sajó, A. Horváth, Impregnated Ni/ZrO2 and Pt/ZrO2 catalysts in dry reforming of methane: Activity tests in excess methane and mechanistic studies with labeled 13CO2, Applied Catalysis A: General 504 (2015) 608-620.

[47] Y. Yan, Y. Dai, H. He, Y. Yu, Y. Yang, A novel W-doped Ni-Mg mixed oxide catalyst for CO2 methanation, Applied Catalysis B: Environmental 196 (2016) 108-116.

[48] X. Jiao, L. Li, N. Zhao, F. Xiao, W. Wei, Synthesis and Low-Temperature CO2 Capture Properties of a Novel Mg–Zr Solid Sorbent, Energy & Fuels 27 (2013) 5407-5415.

[49] H. Lu, X. Yao, J. Li, S. Yao, Z. Wu, H. Zhang, H. Lin, T. Nozaki, Mechanism on the plasma-catalytic oxidation of graphitic carbon over Au/γ-Al2O3 by in situ plasma DRIFTS-mass spectrometer, Journal of Hazardous Materials 396 (2020) 122730.

[50] X. Wang, U.S. Ozkan, Correlation of NO and CO2 adsorption sites with aldehyde hydrogenation performance of sulfided NiMo/Al2O3 catalysts, Journal of Catalysis 227 (2004) 492-501.

[51] R. Snoeckx, A. Bogaerts, Plasma technology - a novel solution for CO2 conversion?, Chemical Society reviews 46 (2017) 5805-5863.

[52] T. Nozaki, N. Muto, S. Kado, K. Okazaki, Dissociation of vibrationally excited methane on Ni catalyst: Part 1. Application to methane steam reforming, Catalysis Today 89 (2004) 57-65.

[53] J. Quan, F. Muttaqien, T. Kondo, T. Kozarashi, T. Mogi, T. Imabayashi, Y. Hamamoto, K. Inagaki, I. Hamada, Y. Morikawa, J. Nakamura, Vibration-driven reaction of CO2 on Cu surfaces via Eley–Rideal-type mechanism, Nature Chemistry 11 (2019) 722-729.

[54] H. Ueta, L. Chen, R.D. Beck, I. Colon-Diaz, B. Jackson, Quantum state-resolved CH4 dissociation on Pt(111): coverage dependent barrier heights from experiment and density functional theory, Physical chemistry chemical physics : PCCP 15 (2013) 20526-20535.

[55] A.S. Al-Fatesh, M.A. Naeem, A.H. Fakeeha, A.E. Abasaeed, Role of La2O3 as Promoter and Support in Ni/γ-Al2O3 Catalysts for Dry Reforming of Methane, Chinese Journal of Chemical Engineering 22 (2014) 28-37.

[56] H.J. Lee, W. Joe, I.K. Song, Direct synthesis of dimethyl carbonate from methanol and carbon dioxide over transition metal oxide/Ce0.6Zr0.4O2 catalysts: Effect of acidity and basicity of the catalysts, Korean Journal

of Chemical Engineering 29 (2012) 317-322.

[57] J. Horlyck, S. Lewis, R. Amal, J. Scott, The Impact of La Doping on Dry Reforming Ni-Based Catalysts Loaded on FSP-Alumina, Topics in Catalysis 61 (2018) 1842-1855.

[58] D. Andriamasinoro, R. Kieffer, A. Kiennemann, J.L. Rehspringer, P. Poix, A. Vallet, J.C. Lavalley, Preparations and characterization of lanthana catalysts: study of their activity in CO/H2 reactions, Journal of Materials Science 24 (1989) 1757-1766.

[59] V. Lochař, FT-IR study of methanol, formaldehyde and methyl formate adsorption on the surface of Mo/Sn oxide catalyst, Applied Catalysis A: General 309 (2006) 33-36.

[60] Q. Yang, X. Yin, C. Wu, S. Wu, D. Guo, Thermogravimetric-Fourier transform infrared spectrometric analysis of CO2 gasification of reed (Phragmites australis) kraft black liquor, Bioresource Technology 107 (2012) 512-516.

[61] C.-J. Liu, B. Xue, B. Eliasson, F. He, Y. Li, G.-H. Xu, Methane Conversion to Higher Hydrocarbons in the Presence of Carbon Dioxide Using Dielectric-Barrier Discharge Plasmas, Plasma Chemistry and Plasma Processing 21 (2001) 301-310.

[62] S. Kameshima, K. Tamura, Y. Ishibashi, T. Nozaki, Pulsed dry methane reforming in plasma-enhanced catalytic reaction, Catalysis Today 256 (2015) 67-75.

[63] T. Nozaki, S. Kameshima, Z. Sheng, K. Tamura, T. Yamazaki, in: X. Tu, J.C. Whitehead, T. Nozaki (Eds.), Plasma Catalysis: Fundamentals and Applications, Springer International Publishing, Cham, 2019, pp. 231-269.

[64] Y. Wu, H. Xie, S. Tian, N. Tsubaki, Y. Han, Y. Tan, Isobutanol synthesis from syngas over K–Cu/ZrO2–La2O3(x) catalysts: Effect of La-loading, Journal of Molecular Catalysis A: Chemical 396 (2015) 254-260.

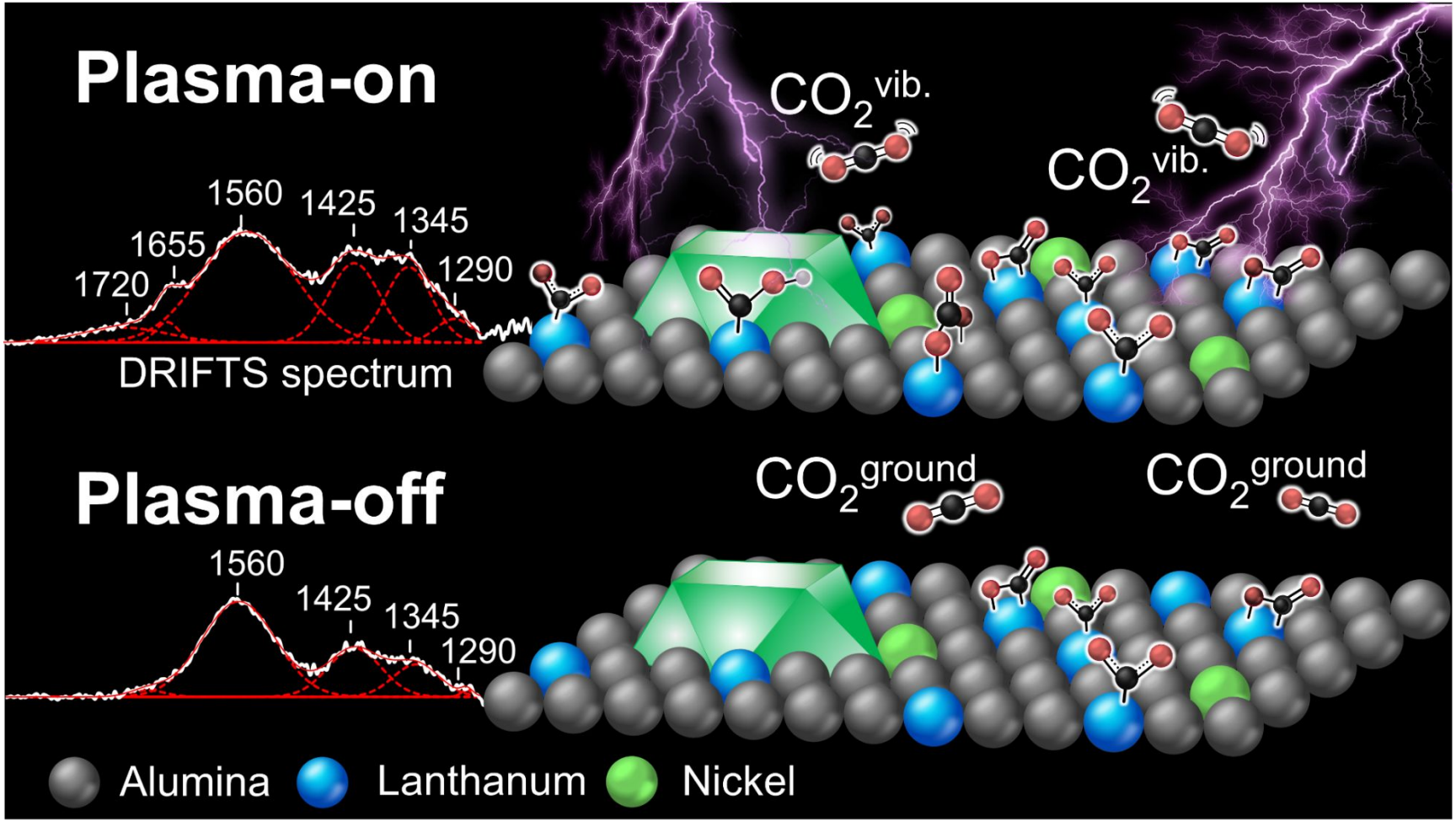

Abundant carbonate species are generated over lanthanum by vibrationally excited CO_2, which increase adsorbed oxygen species fixation for surface reaction.